JCTC Journal of Chemical Theory and Computation

Article

pubs.acs.org/JCTC

Binding in Radical-Solvent Binary Complexes: Benchmark Energies and Performance of Approximate Methods

Peter R. Tentscher[†] and J. Samuel Arey*[,†,‡]

[†]Environmental Chemistry Modeling Laboratory, EPFL, Lausanne, Switzerland

[‡]Swiss Federal Institute of Aquatic Science and Technology (Eawag), Dübendorf, Switzerland

Supporting Information

ABSTRACT: In many situations, weak interactions between radicals and their environment potentially influence their properties and reactivity. We computed benchmark binding energies of 12 binary complexes involving radicals, using basis set extrapolated coupled cluster theory with up to CCSDT(Q) excitations plus corrections for core correlation and relativistic effects. The set was comprised of both electron-rich and electron-poor small radicals which were either neutral or positively charged. The radicals were complexed with the closed-shell polar (model) solvent molecules H_2O and HF. On the basis of these accurate *ab initio* binding energies, we assess the performance of many modern DFT functionals for these radical-solvent molecule interactions. Radical hydrogen bonded complexes are well-described by most DFT methods, but two-center−three-electron interactions are at least slightly overbound by most functionals evaluated here, including range-separated functionals. No such systematic error was found for electron-rich metal−water complexes. None of the functionals tested yield chemical accuracy for all types of complexes.

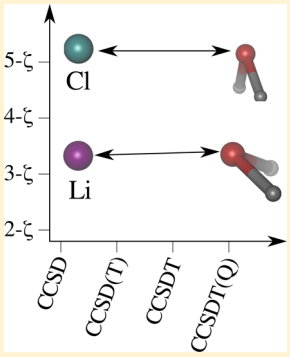

1. INTRODUCTION

Radicals play an important role in many areas of chemistry, such as atmospheric,[1−4] aquatic,[5] polymer,[6] and biological,[7] to name a few. In many environments of practical interest, radicals can interact with closed-shell molecules. In gas phase chemistry, weakly bound pre- and postreactive complexes of radicals can determine the reaction channel followed by the system.[8] Water is suspected to catalyze radical reactions in atmospheric chemistry, either as a single molecule catalyst or by forming microhydrated clusters around the reactants.[9,10] To study solvation phenomena and the dynamics of supermolecular clusters, electron-rich main-group metals are frequently used to dope, for example, $(H_2O)_n$,[11−13] $(NH_3)_n$,[11,14,15] or $(HAc)_n$.[16] In the condensed phase and in microsolvated environments, additional specific interactions with solvent molecules are possible. Weak interactions, such as hydrogen bonds, halogen bonds, or charge-transfer complexes, are known to steer thermodynamics and kinetics in many closed-shell chemical reactions in the condensed phase, for example in the S_N2 reaction.[17] Analogous solvent influences should be expected in reactions involving radicals. In open-shell systems, additional two-center−three-electron interactions can arise, as discussed in more detail below. Hence, the simulation of radical chemistry often requires methods that accurately describe not only the radical itself but also the weak interactions with its environment.

The interactions of radicals with closed-shell molecules differ somewhat from those in closed shell−closed shell complexes. Analogous to closed-shell systems, van der Waals interactions are present. However, an "incipient chemical bond" can arise between a radical and a noble gas atom.[18] Analogous to closed-shell systems, hydrogen bonds to a radical center are possible, as observed for the $HOH\cdots CH_3$ complex[19] or the phenoxyl radical-water complex.[20] Unlike closed-shell systems, radicals can engage in "hemibonded" or "two-center−three-electron bond" interactions.[21] As shown by Bickelhaupt,[22] these interactions can also be interpreted as a one-electron bond plus a Pauli repulsion term. Starting with the work of Gill and Radom,[21] most research on hemibonded systems has focused on cationic homodimeric complexes,[22−25] which have been studied extensively in subsequent articles.

Our research focuses on interactions of radicals with water, as (micro)solvated radicals are of particular interest for oxidative transformations occurring in biological, aquatic, marine, and atmospheric systems. Hobza et al. were the first to report on molecular radical cations complexed by a single water molecule,[26,27] followed by studies on other such complexes.[23,28−30] For these systems, the hemibonded structures represent only local minima on the potential energy surface (PES). The global minima occur as either the radical cation as a hydrogen bond donor or as the corresponding proton-transferred complex. We are aware of one report of a radical cation with a hemibonded structure as the global minimum,[31] in which case the ammonium radical cation is bound to thioformaldehyde *en lieu* of water.

For small radical-molecule complexes, highly accurate *ab initio* binding energies are scarce: for only a few systems have CCSD(T) binding energies been reported,[23,24] and we are unaware of published post-CCSD(T) data for such systems.

Received: October 1, 2012
Published: February 22, 2013

dx.doi.org/10.1021/ct300846m | *J. Chem. Theory Comput.* 2013, 9, 1568−1579

The types of interactions reported above can all be described, in principle, by wave function-based methods. Nonetheless, open-shell systems imply some possible additional problems for wave function methods[32] which can be diagnosed when necessary.[33,34] Accurate thermochemical assessments using wave function theory are limited to small systems, due to the steep scaling of computational cost with system size inherent to these methods. For larger clusters, microhydrated environments, sizable organic molecules, or condensed phase simulations, the type of model used is dictated by the system size. For such systems, density functional theory (DFT) methods may often be the most practical approach.

We are unaware of a systematic assessment of modern DFT methods for a diverse set of radical-solvent intermolecular interactions, possibly due to the lack of reliable benchmark data for complexes of radicals with solvent or solvent-like molecules. Thus far, rigorous testing of DFT methods for radical-molecule complexes has focused upon a few hemibonded complexes, most of which were cationic or anionic homodimeric complexes. For these systems, DFT methods exhibit mixed performances, with many functionals exhibiting significant overbinding.[23,24,35,36] These shortcomings are attributed to the self-interaction error (SIE) inherent to conventional DFT[35,36] or to the inclusion of nondynamical correlation in the exchange functional.[37] In this respect, hemibonded systems behave similarly to closed-shell charge transfer (CT) complexes, for which DFT also exhibits overbinding due to the SIE.[38,39] Two strategies are often used to correct for the SIE: Perdew−Zunger self-interaction correction (SIC)[40−42] and, more recently, long-range corrected density functionals.[43−45] In past studies,[23,24,36,46] functionals with a high fraction of exact exchange were also found to perform favorably for systems in which the SIE is problematic. In this respect, it has been suggested that functionals parametrized with pure exact exchange may overcome the problems in describing hemibonded systems.[36]

In the present work, we address the following questions: (a) What range of binding energies is explored by complexes of radicals with polar solvent molecules? (b) Is CCSD(T) a sufficient tool for their description? (c) Can existing DFT methods sufficiently describe all different types of radical−solvent binding?

We report *ab initio* binding energies for radical−solvent complexes that are prototypical for condensed phase chemistry in polar solvents: a radical is allowed to interact with water or hydrogen fluoride as a model solvent. We intentionally focus upon interactions that directly involve the unpaired electron, although these conformations may not represent the global minima of the respective complexes. We considered the following binding situations:

- Neutral and cationic electron-poor/hemibonded complexes
- Neutral and cationic complexes of water with electron-rich main group metal radicals
- Hydrogen bonding with the radical center as hydrogen bond acceptor
- Hydrogen bonding with the acidic proton of a radical cation as hydrogen bond donor

For 12 model complexes, we located minima on an all-electron CCSD(T)/aug-cc-pVTZ potential energy surface (PES). On selected stationary points, we compute basis-set extrapolated (CBS) CCSD(T) binding energies with additional corrections for core−valence correlation, up to CCSDT(Q) excitations, and relativistic effects. Using these binding energies, we evaluate the performance of a number of DFT functionals. We did not consider complexes involving anionic radicals.

2. METHODS

2.1. Selection of Model Complexes. We considered a set of 12 open shell model complexes that contains cationic ($HF\cdots CO^+$, $H_2O\cdots NH_3^+$, $H_2O\cdots HNH_2^+$, $H_2O\cdots Be^+$) as well as neutral ($H_2O\cdots F$, $H_2O\cdots Cl$, $H_2O\cdots Br$, $H_2O\cdots Li$, $H_2O\cdots Al$, $HOH\cdots CH_3$, $FH\cdots BH_2$, $FH\cdots NH_2$, $FH\cdots OH$) doublet radicals. Minima were searched and confirmed on a CCSD(T)/aug-cc-pVTZ potential energy surface. The optimized structures do not necessarily correspond to global minima but to conformations where the unpaired electron is oriented toward the binding partner. These complexes were selected in order to include a variety of binding situations involving the unpaired electron. Spin contamination of the UHF reference was negligible ($\langle S^2\rangle \leq 0.76$) in most cases, with the exceptions of Al ($\langle S^2\rangle = 0.77$) and CO^+ ($\langle S^2\rangle = 0.97$) as well as the corresponding complexes $H_2O\cdots Al$ ($\langle S^2\rangle = 0.79$) and $HF\cdots CO^+$ ($\langle S^2\rangle = 0.86$).

2.2. Coupled Cluster Geometries and Benchmark Binding Energies. HF,[47] CCSD,[48] EOMIP-CCSD,[49] EOMEA-CCSD,[50] and CCSD(T)[51] calculations were conducted with the CFOUR v1[52] electronic structure program. CCSDT,[53] CCSDT(Q),[54] and CCSDTQ[55] calculations were conducted with the MRCC[56] program linked to CFOUR v1. Dunning's correlation consistent basis sets[57−62] were used throughout. In some calculations, the aug-cc-pVXZ (X = D,T,Q,5) bases were used on p-block elements together with cc-pVXZ bases on H, Li, and Be. This is referred to as aug′-cc-pVXZ in the remainder of the manuscript. We used UHF references for most open-shell calculations. The U prefix is dropped in the remainder of the manuscript, and ROHF-based methods are prefixed with RO.

Benchmark geometries were computed at the all-electron (AE)-CCSD(T)/aug-cc-pVTZ level of theory in most cases. For CO^+ and $HF\cdots CO^+$, ROHF references were employed. For $H_2O\cdots Li$, AE-CCSD(T)/aug-cc-pCVTZ was used instead of AE-CCSD(T)/aug-cc-pVTZ. We considered this necessary because the optimization of the $H_2O\cdots Li$ complex with AE-CCSD(T)/aug-cc-pVTZ produced a C_{2v} geometry, whereas optimization with AE-CCSD(T)/aug-cc-pCVTZ produced a C_S geometry. In the remainder of the manuscript, we refer to the AE-CCSD(T)/aug-cc-pCVTZ geometry of $H_2O\cdots Li$ and the other AE-CCSD(T)/aug-cc-pVTZ geometries collectively as "AE-CCSD(T)/aug-cc-pVTZ." Geometries were optimized by converging the root mean squared forces to 10^{-8} Hartree per Bohr. Additionally, frozen-core (FC-)CCSD/aug-cc-pVTZ and FC-CCSD/aug-cc-pVDZ geometries were computed. EOMIP-CCSD/aug-cc-pVTZ geometry optimizations were conducted for complexes containing F, Cl, Br, NH_3^+, CO^+, BH_2, NH_2, and OH, as well as EOMEA-CCSD/aug-cc-pVTZ calculations for complexes containing Li, Be^+, Al, and CH_3.

All optimized geometries described above were confirmed to be true minima by harmonic frequency calculations. These were performed using analytical second derivatives[63] with the CCSD and CCSD(T) methods, and using numerical second derivatives of analytical gradients for ROCCSD(T) and for the EOMIP or EOMEA formalisms. Additionally, VPT2[64] calculations were performed for some complexes at the CCSD/aug-cc-pVDZ, EOMIP-CCSD/aug-cc-pVDZ, and EOMEA-

CCSD/aug-cc-pVDZ levels of theory, with the frozen core approximation applied throughout.

Following a suggestion of one of the reviewers, we evaluated whether core−valence basis functions and basis-set superposition error (BSSE) could contribute significant errors to the AE-CCSD(T)/aug-cc-pVTZ geometries. We performed additional geometry optimizations with the AE-CCSD(T)/aug-cc-pCVQZ model chemistry, for which core−valence basis functions are included, and for which basis set incompleteness/superposition should only play a minor role. Normal mode analysis was not performed. In addition, in order to further evaluate the possible importance of counterpoise correction, MP2 geometry optimizations were performed with Gaussian 09 rev. B.1,[65] using "very tight" energy and geometry convergence criteria. These were all-electron calculations with the aug-cc-pVTZ, aug-cc-pCVTZ, and aug-cc-pwCVQZ basis sets, as well as frozen-core calculations with the aug-cc-pVTZ basis. All MP2 calculations were performed both with and without employing the counterpoise correction[66,67] during the geometry optimization.

We evaluated benchmark binding energies on the AE-CCSD(T)/aug-cc-pVTZ benchmark geometries, where the complete nonrelativistic binding energy is given by

$$E_{\text{nonrel}} = E_{\text{CCSD(T)/CBS}} + \Delta E_{\text{core}} + \Delta E_{\text{HLC}} \quad (1)$$

To evaluate the basis set extrapolated frozen-core CCSD(T) energy, $E_{\text{CCSD(T)/CBS}}$, the HF, CCSD, and (T) components of the CCSD(T) energies were extrapolated separately to the complete basis set (CBS) limit:

$$E_{\text{CCSD(T)/CBS}} = E_{\text{HF/CBS}} + \Delta E_{\text{CCSD/CBS}} + \Delta E_{\text{(T)/CBS}} \quad (2)$$

We considered different extrapolation formulas for the correlation energies, including those of Halkier et al.[68] and Schwenke.[69] Among these, we found the difference in results for the final binding energies to be <0.05 kJ/mol. Here, we report results from the two point extrapolation proposed by Schwenke[69] with the aug′-cc-pV(Q,5)Z bases, but we employ the extrapolation coefficients optimized for the aug-cc-pVXZ bases. We found that using the published coefficients previously optimized for either aug-cc-pVXZ or cc-pVXZ resulted in binding energy differences of <0.01 kJ/mol. Hence, we inferred that the uncertainty resulting from the use of nonoptimized coefficients remains well below the expected limits of accuracy of this study. The core correlation contribution (ΔE_{core}) and the frozen-core post-CCSD(T) correction (ΔE_{HLC}) terms were computed as

$$\Delta E_{\text{core}} = E^{\text{all-electron}}_{\text{CCSD(T)/aug-cc-pCVQZ}} - E^{\text{frozen-core}}_{\text{CCSD(T)/aug-cc-pCVQZ}} \quad (3)$$

$$\Delta E_{\text{HLC}} = \Delta E_{\text{T}} + \Delta E_{\text{(Q)}} \quad (4)$$

$$\Delta E_{\text{T}} = E_{\text{CCSDT/cc-pVTZ}} - E_{\text{CCSD(T)/cc-pVTZ}} \quad (5)$$

$$\Delta E_{\text{(Q)}} = E_{\text{CCSDT(Q)/cc-pVDZ}} - E_{\text{CCSDT/cc-pVDZ}} \quad (6)$$

For the case of HF···CO^+, $\Delta E_{\text{(Q)}}$ was replaced by ΔE_{Q}, defined as

$$\Delta E_{\text{Q}} = E_{\text{CCSDTQ/cc-pVDZ}} - E_{\text{CCSDT/cc-pVDZ}} \quad (7)$$

because CCSDT(Q) calculations with ROHF references are unavailable in the MRCC implementation. For H_2O···Br, the aug-cc-pwCVQZ basis was used to evaluate ΔE_{core}, and the K-shell of Br was kept frozen.

To calculate a relativistic (real) binding energy, excluding vibrational contributions, we add scalar relativistic effects (ΔE_{SR}) and spin−orbit corrections (ΔE_{SO}) to the binding energy:

$$E_{\text{rel}} = E_{\text{nonrel}} + \Delta E_{\text{SR}} + \Delta E_{\text{SO}} \quad (8)$$

Scalar relativistic (SR) effects were considered using two-electron Mass-Velocity-Darwin (MVD2[70,71]) with all-electron CCSD(T), and the uncontracted cc-pCVQZ basis as

$$\Delta E_{\text{SR}} = E^{\text{MVD2}}_{\text{CCSD(T)/unc-cc-pCVQZ}} - E_{\text{CCSD(T)/unc-cc-pCVQZ}} \quad (9)$$

For all complex and monomer systems containing Li, Be, and Al, a frozen core calculation with the cc-pV5Z basis was used for the scalar relativistic contributions instead. We estimated ΔE_{SO} with DFT calculations at the BHandHLYP/aug-cc-pVQZ level of theory together with the ZORA[72] formalism as implemented in NWChem 6.0,[73] using spin−orbit DFT calculations:[74]

$$\Delta E_{\text{SO}} = E^{\text{spin-orbit}}_{\text{ZORA/DFT}} - E^{\text{scalar-relativistic}}_{\text{ZORA/DFT}} \quad (10)$$

Binding energies were calculated as $E_{\text{bind}} = E_{\text{A···B}} - (E_{\text{A}} + E_{\text{B}})$ by using the respective optimized geometries. Reported binding energies thus implicitly include the deformation of the fragments to their geometries in the supersystem. All calculations were performed without correcting for BSSE. For binding energies of H-bonded systems, it has been shown[75−77] that the BSSE corrections are <0.2 kJ/mol for quadruple-ζ-pentuple-ζ extrapolated CCSD(T) energies. From our frozen core results, we found that the CCSD(T) binding energies are essentially converged with the aug′-cc-pVQZ basis set. Hence, we considered a BSSE correction unnecessary for either frozen-core or core-correlated results. Finally, observing that post-CCSD(T) contributions were small, we did not further converge them in terms of basis set size.

2.3. Density Functional Theory Calculations. Most DFT calculations with atom-centered basis functions were conducted with the Gaussian 09 rev. B.1[65] electronic structure program, applying a pruned (99,590) integration grid. "Tight" (or better) energy and geometry convergence criteria were used throughout. DFT single point calculations were conducted with the aug-cc-pVQZ basis, using structures previously optimized at the AE-CCSD(T)/aug-cc-pVTZ level of theory. In separate calculations, structures were also optimized at the DFT/aug-cc-pVDZ level of theory, which was followed by vibrational analysis and single point calculations at the DFT/aug-cc-pVQZ level of theory. Selected DFT methods were used: BLYP,[78] B3LYP,[79] B2PLYP,[80] B2PLYP-D,[81] M062X,[82] M06HF,[83] BMK,[84] PBE,[85,86] BHandH,[87] BHandHLYP,[87] MPW1K,[88] and MPW2PLYP.[89] Long-range corrected calculations were conducted with the CAM-B3LYP,[44] ωB97,[90] ωB97X,[90] ωB97X-D,[91] and LC-ωPBE[92] methods, as well as by applying Hirao's long-range correction[45] to the pure BLYP and PBE functionals. We refer to these results using the prefix "LC-". All calculations were performed without correcting for BSSE, because the DFT binding energies were found to be well-converged with the aug-cc-pVQZ basis based on comparison to aug-cc-pVTZ results.

Additional DFT calculations were conducted with the Q-Chem 4.0[93] electronic structure program, and an unpruned

(99,590) integration grid was used. Energies using the aug-cc-pVQZ basis on the CCSD(T) benchmark structures were calculated with the M11,[94] XYG3,[95] and ωB97X-2[96] (in its parametrization for the CBS limit as implemented in Q-Chem) functionals, employing a DIIS convergence of at least 10^{-9} Hartree.

Gaussian-augmented plane wave (GPW) DFT calculations were conducted with the CP2K[97] electronic structure program. We used a cubic, nonperiodic box of 25 × 25 × 25 Å with a 300 Ry plane-wave cutoff. The BLYP functional with restricted open shell orbitals was used with GTH pseudopotentials[98] and the corresponding QZV2P basis. Exceptions are Br, where the MOLOPT-DZVP basis was used instead (as larger basis sets were unavailable), and Be, where the DZVP basis was used due to convergence problems with larger basis sets. These calculations are referred to as GPW-BLYP. In separate calculations, Mauri's self-interaction correction (SIC)[42] was applied to the spin density, by using a coulomb-scaled approach introduced by VandeVondele and Sprik[41] with scaling parameters of a = 0.2 and b = 0.0. This is referred to as GPW-BLYP-SIC below. In additional calculations, Grimme's dispersion correction[99] was added, and this is referred to as GPW-BLYP-SIC-D.

2.4. Additional Wave Function Methods. On the AE-CCSD(T)/aug-cc-pVTZ benchmark geometries, additional wave function single point energies using the aug-cc-pVQZ basis were conducted as follows. Frozen-core MP2,[48] ROMP2, and (U)CCSD calculations were performed with Gaussian 09. Frozen-core CC2[100] calculations were performed with CFOUR v1. All-electron spin-opposite scaled RI-MP2 calculations were performed with Q-Chem 4.0, employing a scaling factor of 1.0 (SOS-MP2[101]) and also employing optimized orbitals (O2-MP2[102]).

3. RESULTS AND DISCUSSION

3.1. CCSD(T) Benchmark Geometries. We defined benchmark geometries as those optimized at the AE-CCSD(T)/aug-cc-pVTZ level of theory, and these are depicted in Figure 1. We have recently shown[34] that CCSD(T) calculations based on UHF references yield geometries of high quality for small radicals. However, additional uncertainties may arise for complexes, including BSSEs. To evaluate the accuracy of the AE-CCSD(T)/aug-cc-pVTZ geometries, we computed additional geometries with the aug-cc-pCVQZ basis for most systems. The resulting interfragment distances of these geometries are given in Figure 1, alongside the distance of the benchmark geometries. If we assume the AE-CCSD(T)/aug-cc-pCVQZ geometries to be basis-set converged, then the error in interfragment distances of the AE-CCSD(T)/aug-cc-pVTZ geometries due to basis set effects is ≤1.5 pm for all complexes (Table S3). As we discuss in section 3.2, these errors negligibly affect the computed binding energies.

To gain additional insight into the possible importance of counterpoise correction and core−valence basis functions, we conducted AE-MP2 geometry optimizations with the aug-cc-pVTZ, aug-cc-pCVTZ, and aug-cc-pwCVQZ basis sets, as well as FC-MP2 geometry optimizations with the aug-cc-pVTZ basis, all with and without using the counterpoise correction during the geometry optimization. The results of these calculations suggest that there is error cancellation between the BSSE, basis-set incompleteness, and the absence of core−valence functions (Table S2). This may rationalize why AE-CCSD(T)/aug-cc-pVTZ geometries are found to be in very close agreement with the more rigorous AE-CCSD(T)/aug-cc-pCVQZ geometries. MP2 interfragment distances are shown in Table S2, and differences in interfragment distances between aug-cc-pVTZ geometries and the respective best quadruple-ζ geometries are shown in Table S3, for both AE-MP2 and AE-CCSD(T).

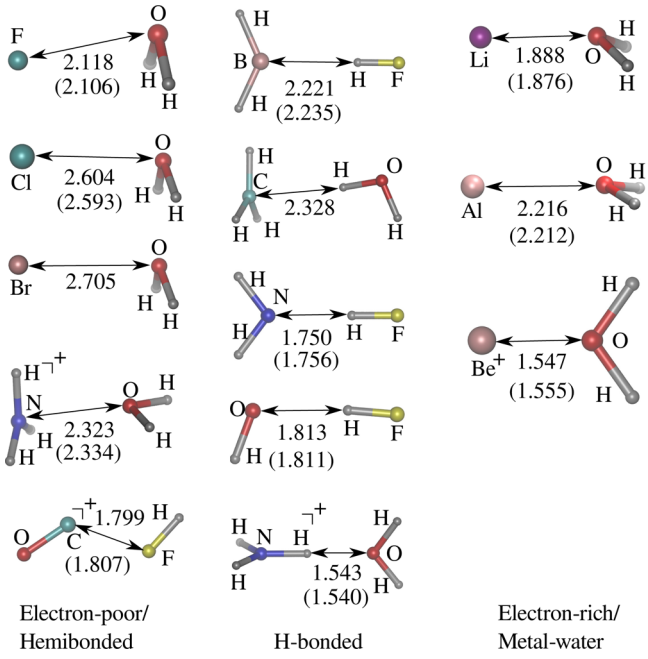

Figure 1. Geometries of complexes optimized with all-electron CCSD(T)/aug-cc-pVTZ. The shortest internuclear distances between the fragments are given [Å]; distances of AE-CCSD(T)/aug-cc-pCVQZ geometries are given in parentheses.

3.2. Benchmark Binding Energies. All benchmark binding energies were calculated using the AE-CCSD(T)/aug-cc-pVTZ benchmark geometries. The total nonrelativistic binding energy (E_{nonrel}) was evaluated as the sum of $E_{HF/CBS}$, ΔE_{CCSD}, $\Delta E_{(T)}$, ΔE_{core}, and ΔE_{HLC} (eqs 1 and 2). This is our best estimate of the nonrelativistic binding energy, which is used for evaluating DFT methods in section 3.3. In order to obtain a best estimate of the relativistic binding energy (E_{rel}), we add scalar relativistic contributions (ΔE_{SR}) and spin−orbit contributions (ΔE_{SO}) to E_{nonrel}. We also report harmonic zero-point vibrational energy corrections based on AE-CCSD(T)/aug-cc-pVTZ frequencies (ΔE_{ZPVE}^{harm}). For some systems, we additionally report anharmonic corrections to the ZPVE, which are computed with the VPT2 formalism at the FC-CCSD/aug-cc-pVDZ level of theory. All energy contributions for all complexes are reported in Table 1.

For most of the systems considered here, the nonrelativistic benchmark binding energy is reproduced by FC-CCSD(T)/CBS to within 1 kJ/mol. However, core correlation is significant for the complexes containing heavy elements (Al, Cl, Br), or group 1 and 2 metals (Li, Be), and, surprisingly, also for HF···CO^+. Post-CCSD(T) excitations are mildly important (<1 kJ/mol) for the hemibonded systems (first section of Table 1), which may be indicative of a slight nondynamical correlation contribution to the binding in these systems.[34] For the HF···CO^+ complex, for which the data in Table 1 are based on ROHF references, we conducted additional non-relativistic calculations based on the (spin-contaminated) UHF reference. The ROHF- and UHF-based binding energies differ

dx.doi.org/10.1021/ct300846m | J. Chem. Theory Comput. 2013, 9, 1568−1579

Table 1. Benchmark Binding Energy Components [kJ/mol], Evaluated at AE-CCSD(T)/aug-cc-pVTZ Geometries

energy component	$E_{HF/CBS}$	$\Delta E_{CCSD/CBS}$	$\Delta E_{(T)/CBS}$	ΔE_{core}	ΔE_T	$\Delta E_{(Q)}$	E_{nonrel}[a]	ΔE_{SR}	ΔE_{SO}	E_{rel}[b]	ΔE_{ZPVE}^{harm}	ΔE_{ZPVE}^{VPT2}
electron-poor/hemibonded complexes												
$H_2O\cdots NH_3^+$	−57.06	−16.09	−2.94	−0.26	−0.35	−0.07	−76.76	0.11	0.00	−76.65	9.08	
$H_2O\cdots F$	27.55	−35.67	−7.05	0.07	−0.69	−0.23	−16.02	0.00	0.00	−16.03	4.82	−0.61
$H_2O\cdots Cl$	5.84	−16.84	−3.84	−0.39	−0.12	−0.10	−15.44	−0.20	0.22	−15.42	3.76	−0.38
$H_2O\cdots Br$	5.62	−16.28	−3.48	−0.43	−0.06	−0.10	−14.73	−0.37		−15.11	3.50	−0.39
$HF\cdots CO^+$[c]	−85.43	−30.93	−5.41	−0.46	0.27	−0.09	−122.04	−0.16	0.00	−122.20	7.43	−0.39
H-bonded complexes												
$H_2O\cdots HNH_2^+$	−88.48	−10.12	−1.67	−0.35	−0.02	−0.10	−100.74	0.14	0.00	−100.61	7.64	
$FH\cdots BH_2$	−7.54	−7.87	−1.33	−0.08	−0.04	−0.03	−16.89	0.00	0.00	−16.89	8.56	−0.66
$HOH\cdots CH_3$	−0.01	−5.86	−1.12	−0.03	−0.02	−0.03	−7.07	−0.06	0.00	−7.13	5.67	
$FH\cdots NH_2$	−32.43	−6.78	−1.60	−0.29	0.00	−0.06	−41.16	0.13	0.00	−41.03	12.35	−0.86
$FH\cdots OH$	−17.80	−5.59	−1.30	−0.09	−0.03	−0.05	−24.86	0.07		−24.80	7.88	−0.65
electron-rich/metal−water complexes												
$H_2O\cdots Li$	−41.75	−7.26	−0.69	−1.95	−0.11	−0.05	−51.82	0.05	0.00	−51.77	4.28	
$H_2O\cdots Al$	−16.29	−11.08	−3.80	−0.41	0.03	−0.21	−31.76	0.20	0.00	−31.56	3.03	
$H_2O\cdots Be^+$	−263.58	−1.77	0.95	−4.10	−0.13	0.01	−268.62	0.31	0.00	−268.31	9.83	−0.15

[a]Total nonrelativistic binding energy. [b]Total relativistic binding energy. [c]Calculations based on ROHF references.

by 0.3 kJ/mol at the CCSD/CBS level, by 1.6 kJ/mol at the CCSD(T)/CBS level, and by 0.3 kJ/mol after the HLC correction (which amounts to 2.1 kJ/mol in the UHF case). This indicates that for the $HF\cdots CO^+$ complex, (a) the perturbative triples treatment is especially prone to an imperfect reference[32] and (b) that post-CCSD(T) contributions can correct for these imperfections efficiently.

As expected, relativistic effects are most pronounced for the complexes which contain second- and third row elements. However, scalar relativistic effects contribute less than 1 kJ/mol to the binding energy in all cases. For $H_2O\cdots Br$ and $FH\cdots OH$, we do not report ΔE_{SO}: for these cases, the ΔE_{SR} computed by the ZORA/DFT scheme deviates substantially from the MVD2/CCSD(T) results, and consequently we considered the computed ΔE_{SO} values from the ZORA/DFT scheme to be unreliable. For the remaining systems, our diagnostics suggest that spin−orbit effects play only a small role.

Our results agree well with previously reported *ab initio* binding energy data. For the two conformations of $H_2O\cdots NH_3^+$, our frozen-core CCSD(T)/CBS results are within 0.5 kJ/mol of the CCSD(T)/CBS//CCSD(T)/aug-cc-pVDZ results of Kim and Lee.[23] For $H_2O\cdots Br$ and $H_2O\cdots Cl$, our CCSD(T)/CBS results are within 1 kJ/mol of the best estimates of Shepler et al.[103] For the $HOH\cdots CH_3$ complex, our ZPVE corrected result is 1.6 kJ/mol lower than the MP2/aug-cc-pVTZ results of Rudić et al.[19]

We estimate the uncertainty in the nonrelativistic binding energy (not corrected for vibrational contributions) to be on the order of 1 kJ/mol, as follows. In order to obtain an upper limit of the uncertainty, we considered the available literature data on atomization energies of small molecules. Helgaker et al.[104] expect the basis set error in atomization energies, evaluated with AE-CCSD(T)/cc-pCV{Q5}Z extrapolated results, to be <0.7 kJ/mol. They report the mean absolute error and the maximum deviation for evaluating core correlation with the cc-pCVQZ basis, relative to cc-pCV5Z results, to be 0.2 and 0.4 kJ/mol, respectively. For ΔE_T, Karton et al.[105] report that the contribution to the atomization energy is converged to within <0.5 kJ/mol when using a triple ζ basis. For the $\Delta E_{(Q)}$ contribution to the atomization energy, the results of Karton suggest that the basis set errors when using the cc-pVDZ basis are on the order of 1 kJ/mol, but these errors can be up to 3 kJ/mol in some cases. However, the contribution of $\Delta E_{(Q)}$ to the binding energy in our results is ≤0.26 kJ/mol for two cases and <0.1 kJ/mol for the remaining cases. Also, ΔE_T is similar in magnitude compared to $\Delta E_{(Q)}$ in all cases. The observed energy components $E_{CCSD(T)/CBS}$, ΔE_{core}, ΔE_T, and $\Delta E_{(Q)}$ are "small" for the binding energies of our weak isogyric complexes, compared to the atomization energies studied in the above reports, where covalent bonds are broken and formed. Hence, we estimate the error in the binding energies caused by basis-set incompleteness of the individual components to be <1 kJ/mol overall.

Despite that we have recently shown[34] that geometries of molecular radicals derived with all-electron CCSD(T)/aug-cc-pVTZ qualify for thermochemical calculations in the (sub-)kJ/mol range, these geometries may, in principle, be a source of significant energetic error in computed binding energies of complexes. To estimate the energetic errors arising from basis set incompleteness of the benchmark geometries, we calculated the binding energies at the AE-CCSD(T)/aug-cc-pCVQZ level of theory using both the AE-CCSD(T)/aug-cc-pVTZ and the AE-CCSD(T)/aug-cc-pCVQZ geometries. The resulting difference in binding energy was considered indicative of the energetic error inherent in the CCSD(T)/aug-cc-pVTZ benchmark geometries. For the worst cases, $H_2O\cdots F$ and $H_2O\cdots Cl$, differences in binding energy amount to −0.07 kJ/mol and −0.05 kJ/mol, respectively. The complete list of these estimated uncertainties (which can be interpreted as corrections to the calculated benchmark binding energies) are given in the SI (Table S1). Note that although these energetic discrepancies may be considered relevant for the interpretation of calculated absolute binding energies, they are not relevant for the assessment of DFT binding energies that we report in section 3.3; both the DFT calculations and the benchmark binding energies use identical geometries.

The uncertainties in the ZPVE corrections to the binding energies are more difficult to estimate. UHF references can bear near-instabilities or true instabilities,[32,106] which can especially affect CCSD(T) second derivative calculations. However, these problems are less prominent at the CCSD level and are absent when using the EOMIP or EOMEA formalisms.[32,34] For all of our calculations, structures and harmonic frequencies are in good agreement between CCSD(T), CCSD, and EOMIP/

Table 2. Errors in Binding Energies Using Different Wave Function and DFT Methods (aug-cc-pVQZ Basis) with Respect to the Nonrelativistic Coupled Cluster Benchmark Binding Energies (As Given in First Row) [kJ/mol], Ordered by Method Family and Ascending $\sqrt{\Delta^2}$

	electron-poor/hemibonded complexes					H-bonded complexes					metal−water complexes		
	$H_2O\cdots NH_3^+$	$H_2O\cdots F$	$H_2O\cdots Cl$	$H_2O\cdots Br$	$HF\cdots CO^+$	$H_2O\cdots HNH_2^+$	$FH\cdots BH_2$	$HOH\cdots CH_3$	$FH\cdots NH_2$	$FH\cdots OH$	$H_2O\cdots Li$	$H_2O\cdots Al$	$H_2O\cdots Be^+$
benchmark B.E.	−76.8	−15.9	−15.4	−14.7	−122.04	−100.7	−16.9	−7.1	−41.2	−24.8	−51.8	−31.8	−268.6
approximate wave function methods													
CCSD	3.6	7.0	4.7	2.1	5.9	1.7	1.1	0.8	1.2	0.8	2.8	5.0	4.1
CC2	2.5	9.0	2.5	2.3	−4.3	−0.3	0.6	0.5	−2.1	−0.5	5.3	0.5	7.3
O2-MP2	4.7	9.0	4.4	0.1	6.1	4.1	1.2	1.1	1.6	1.5	−2.6	−9.8	2.6
ROMP2	4.5	16.4	3.0	−0.5	−0.3	−0.5	0.1	−0.2	−1.3	−0.4	6.1	0.1	10.0
MP2	4.5	15.1	3.1	−0.4	−21.5	−0.4	0.2	0.0	−1.4	−0.4	6.1	2.1	10.0
SOS-MP2	8.6	21.4	7.4	2.3	−23.8	3.8	1.7	1.4	1.9	1.8	−2.1	−7.0	1.8
HF	19.6	40.6	21.3	20.3	42.7	12.1	9.2	7.0	8.5	7.3	10.0	15.7	5.2
double hybrid functionals													
XYG3	3.8	5.1	3.9	1.7	−5.5	−1.6	−1.3	0.1	−2.5	−1.3	−3.6	−6.2	−4.0
ωB97X-2	−2.4	−0.1	−2.6	−4.1	−17.7	−2.6	−4.6	−2.7	−3.5	−2.5	−1.3	−12.0	0.2
B2PLYP	−4.6	−11.1	−2.9	−2.1	−20.9	−1.4	−1.6	0.9	−1.2	−0.7	−2.6	2.8	0.9
MPW2PLYP	−6.0	−10.2	−4.0	−3.4	−22.7	−3.6	−2.9	−0.5	−3.3	−2.5	−5.7	0.2	−3.6
B2PLYPD	−7.4	−12.4	−4.6	−4.1	−22.1	−3.8	−3.0	−1.3	−2.8	−2.0	−5.6	0.6	0.0
hybrid functionals													
MPW1K	−1.0	0.4	0.4	1.1	−21.6	−3.5	−0.8	1.9	−1.5	0.3	0.8	−1.6	−7.2
M062x	−6.9	−5.6	−5.1	−3.8	−15.8	−3.6	−3.4	−3.6	−1.4	−1.1	−4.4	−6.4	−6.6
BhandHLYP	−1.5	2.2	1.7	2.5	−21.0	−2.6	−1.0	1.6	−1.9	−0.9	−5.0	3.3	−8.5
M06HF	−2.8	14.1	1.8	0.3	−10.2	−6.9	−2.9	−3.7	−4.4	−0.2	-[a]	−11.6	−5.1
BMK	−5.3	−13.4	−4.1	−1.5	−28.6	0.9	−0.2	2.3	0.6	1.0	6.2	2.2	3.3
B3LYP	−13.3	−32.6	−9.2	−5.2	−34.8	−2.3	−2.6	1.4	−0.8	−0.6	−7.0	3.9	−3.1
BhandH	−20.7	−22.1	−16.0	−15.2	−50.8	−22.5	−9.6	−6.0	−17.3	−13.0	−19.6	−20.5	−30.2
long-range corrected functionals													
M11	−6.7	−7.2	−1.6	−3.0	−24.4	−5.5	0.1	1.1	−2.5	−1.4	5.2	−2.6	1.1
LC-ωPBE	−1.8	−12.7	2.4	3.1	−27.2	−2.2	−0.9	2.3	−1.0	1.1	6.4	−0.7	−5.6
ωB97XD	−10.5	−18.9	−7.4	−5.7	−29.8	−3.3	−3.0	−1.5	−1.3	−0.2	9.5	0.0	17.3
ωB97X	−11.7	−20.8	−9.6	−8.7	−35.3	−4.8	−6.1	−3.2	−4.6	−3.7	11.0	−4.2	17.1
LC-PBE	−7.9	−17.1	−2.1	−1.9	−38.7	−12.4	−3.5	0.2	−8.5	−4.4	0.8	−8.6	−17.6
CAM-B3LYP	−11.4	−25.9	−5.9	−3.4	−38.0	−6.5	−3.7	0.2	−4.6	−3.3	−5.9	0.3	−9.7
ωB97	−12.3	−21.7	−9.3	−9.3	−41.8	−4.5	−6.4	−3.0	−5.1	−4.2	11.2	−3.9	19.4
LC-BLYP	−12.5	−23.9	−4.6	−3.7	−42.9	−13.3	−5.8	−1.8	−10.8	−7.5	−8.0	−5.2	−20.9
GGAs with and without SIC													
GPW-BLYP-SIC	3.8	−3.4	−1.7	2.7	−14.7	2.1	9.8	4.3	−1.0	−17.0	3.1	9.0	−18.3
GPW-BLYP-SIC-D	−2.3	−6.2	−5.3	−1.7	−17.4	−3.2	6.5	−0.4	−4.6	−19.9	−3.4	4.2	−20.2
GPW-BLYP	−22.6	−66.0	−21.1	−10.3	−49.5	−0.7	5.4	1.8	0.2	−16.6	−5.0	5.6	−24.7
BLYP	−25.8	−63.4	−19.8	−12.4	−42.3	−0.3	−3.1	1.8	0.8	−0.6	−9.1	6.3	3.1
PBE	−29.6	−66.1	−25.8	−18.8	−49.7	−6.6	−6.4	−1.8	−4.2	−4.2	−8.8	−5.9	−3.8

[a]Calculation nonconvergent for M06HF.

dx.doi.org/10.1021/ct300846m | J. Chem. Theory Comput. 2013, 9, 1568−1579

Table 3. Error Statistics for Binding Energies of Different Wave Function and DFT Methods [kJ/mol], Organized by Type of Complex

	complete set from Table 2					H-bonded complexes[a]					electron-poor/hemibonded complexes[b]					metal−water complexes[c]				
	$\bar{\Delta}$	σ	$\overline{\lvert\Delta\rvert}$	$\sqrt{\overline{\Delta^2}}$	$\sqrt{\overline{(\%\Delta^2)}}$	$\bar{\Delta}$	σ	$\overline{\lvert\Delta\rvert}$	$\sqrt{\overline{\Delta^2}}$	$\sqrt{\overline{(\%\Delta^2)}}$	$\bar{\Delta}$	σ	$\overline{\lvert\Delta\rvert}$	$\sqrt{\overline{\Delta^2}}$	$\sqrt{\overline{(\%\Delta^2)}}$	$\bar{\Delta}$	σ	$\overline{\lvert\Delta\rvert}$	$\sqrt{\overline{\Delta^2}}$	$\sqrt{\overline{(\%\Delta^2)}}$
approximate wave function methods																				
CCSD	3.1	2.1	3.1	3.7	16.6	1.1	0.4	1.1	1.2	6.4	4.7	1.9	4.7	5.0	22.8	4.0	1.1	4.0	4.1	9.6
CC2	1.8	3.7	2.9	4.0	17.4	−0.4	1.1	0.8	1.0	4.2	2.4	4.7	4.1	4.9	25.0	4.3	3.5	4.3	5.2	6.2
O2-MP2	1.8	4.6	3.8	4.7	20.3	1.9	1.3	1.9	2.2	8.3	4.9	3.2	4.9	5.6	26.0	−3.3	6.2	5.0	6.0	18.0
ROMP2	2.8	5.3	3.3	5.8	29.3	−0.5	0.5	0.5	0.7	1.9	4.6	6.9	4.9	7.7	42.8	5.4	5.0	5.4	6.8	7.2
MP2	1.3	8.4	5.0	8.2	27.7	−0.4	0.6	0.5	0.7	1.8	0.1	13.4	8.9	12.0	40.3	6.1	4.0	6.1	6.9	8.1
SOS-MP2	1.5	10.0	6.5	9.1	41.3	2.1	1.0	2.1	2.3	10.8	3.2	16.6	12.7	15.2	59.3	−2.4	4.4	3.6	4.4	13.0
HF	16.9	12.2	16.9	20.6	96.9	8.8	2.1	8.8	9.0	53.2	28.9	11.6	28.9	30.7	132.3	10.3	5.3	10.3	11.2	30.7
double hybrid functionals																				
XYG3	−0.9	3.6	3.1	3.6	13.6	−1.3	0.9	1.4	1.6	5.0	1.8	4.2	4.0	4.2	17.5	−4.6	1.4	4.6	4.7	11.9
ωB97X-2	−4.3	5.0	4.3	6.4	19.8	−3.2	0.9	3.2	3.3	21.8	−5.4	7.0	5.4	8.3	14.7	−4.4	6.6	4.5	7.0	21.8
B2PLYP	−3.4	6.2	4.1	6.9	21.7	−0.8	1.0	1.1	1.2	7.2	−8.3	7.9	8.3	10.9	31.0	0.4	2.7	2.1	2.3	5.8
MPW2PLYP	−5.3	5.8	5.3	7.7	22.2	−2.6	1.2	2.6	2.8	10.4	−9.3	8.0	9.3	11.7	31.0	−3.0	3.0	3.2	3.9	6.4
B2PLYPD	−5.3	6.1	5.4	7.9	26.4	−2.6	1.0	2.6	2.7	12.5	−10.1	7.5	10.1	12.1	36.9	−1.7	3.4	2.1	3.3	6.3
hybrid functionals																				
MPW1K	−2.5	6.2	3.2	6.5	9.4	−0.7	2.0	1.6	1.9	12.2	−4.1	9.8	4.9	9.7	8.0	−2.7	4.1	3.2	4.3	3.5
M062X	−5.2	3.7	5.2	5.9	22.9	−2.6	1.3	2.6	2.9	25.0	−7.4	4.8	7.4	8.6	23.1	−5.8	1.2	5.8	5.9	12.7
BhandHLYP	−2.4	6.5	4.1	6.7	11.5	−1.0	1.6	1.6	1.7	10.9	−3.2	10.1	5.8	9.6	12.3	−3.4	6.0	5.6	6.0	8.4
M06HF[a]	−2.6	6.6	5.3	6.9	32.6	−3.6	2.4	3.6	4.2	25.4	0.7	8.8	5.8	7.9	36.8	−8.3	4.6	8.3	9.0	25.9
BMK	−2.8	9.2	5.4	9.2	27.5	0.9	0.9	1.0	1.2	14.9	−10.6	11.0	10.6	14.5	37.7	3.9	2.1	3.9	4.2	7.9
B3LYP	−8.2	12.2	9.0	14.3	61.3	−1.0	1.6	1.5	1.7	11.6	−19.0	13.7	19.0	22.6	89.4	−2.1	5.5	4.7	5.0	10.5
BhandH	−20.3	11.0	20.3	22.9	70.3	−13.7	6.5	13.7	14.9	55.5	−24.9	14.7	24.9	28.2	84.8	−23.4	5.9	23.4	23.9	43.7
long-range corrected functionals																				
M11	−3.6	7.1	4.8	7.7	16.6	−1.6	2.6	2.1	2.8	8.3	−8.6	9.1	8.6	11.9	22.6	1.2	3.9	3.0	3.4	7.5
LC-ωPBE	−2.8	8.7	5.2	8.8	26.2	−0.1	1.8	1.5	1.6	15.2	−7.2	12.8	9.5	13.6	35.7	0.1	6.0	4.2	4.9	7.4
ωB97XD	−4.2	11.6	8.4	12.0	39.2	−1.9	1.3	1.9	2.2	12.7	−14.5	10.0	14.5	17.0	55.9	8.9	8.7	8.9	11.4	11.2
ωB97X	−6.5	12.8	10.8	13.9	48.0	−4.5	1.1	4.5	4.6	27.4	−17.2	11.2	17.2	19.9	65.2	8.0	11.0	10.8	12.0	14.9
LC-PBE	−9.4	10.6	9.5	13.9	34.1	−5.7	4.8	5.8	7.2	16.3	−13.5	15.3	13.5	19.3	46.5	−8.5	9.2	9.0	11.3	16.1
CAM-B3LYP	−9.1	10.9	9.1	13.9	48.6	−3.6	2.4	3.7	4.2	12.9	−16.9	14.6	16.9	21.4	70.3	−5.1	5.0	5.3	6.5	6.9
ωB97	−7.0	14.5	11.7	15.6	49.7	−4.6	1.2	4.6	4.8	27.1	−18.9	13.8	18.9	22.6	68.0	8.9	11.8	11.5	13.1	15.0
LC-BLYP	−12.4	11.3	12.4	16.4	47.8	−7.8	4.5	7.8	8.8	26.8	−17.5	16.3	17.5	22.8	65.3	−11.4	8.4	11.4	13.3	13.7
GGAs with and without SIC																				
GPW-BLYP-SIC	−1.6	9.4	7.0	9.1	32.4	−0.4	10.1	6.8	9.0	48.4	−2.7	7.4	5.3	7.1	13.4	−2.1	14.3	10.1	11.9	17.1
GPW-BLYP-SIC-D	−5.7	8.5	7.3	9.9	29.6	−4.3	9.7	6.9	9.7	40.2	−6.6	6.3	6.6	8.7	22.6	−6.5	12.5	9.3	12.1	9.6
GPW-BLYP	−15.7	21.7	17.6	26.1	125.6	−2.0	8.5	4.9	7.8	34.9	−33.9	23.0	33.9	39.7	181.9	−8.0	15.4	11.8	14.9	12.8
BLYP	−12.7	20.6	14.5	23.5	119.9	−0.3	1.8	1.3	1.7	14.2	−32.7	20.4	32.7	37.5	175.7	0.1	8.1	6.2	6.6	15.3
PBE	−17.8	20.1	17.8	26.3	131.2	−4.7	2.0	4.7	5.0	22.4	−38.0	19.5	38.0	41.8	191.7	−6.2	2.5	6.2	6.5	14.6

[a] $H_2O\cdots HNH_2^+$, $FH\cdots BH_2$, $HOH\cdots CH_3$, $FH\cdots NH_2$, $FH\cdots OH_2$. [b] $H_2O\cdots NH_3^+$, $H_2O\cdots F$, $H_2O\cdots Cl$, $H_2O\cdots Br$, $HF\cdots CO^+$. [c] $H_2O\cdots Li$, $H_2O\cdots Be^+$, $H_2O\cdots Al$.

dx.doi.org/10.1021/ct300846m | J. Chem. Theory Comput. 2013, 9, 1568−1579

EOMEA-CCSD. This suggests that the CCSD(T) geometries and harmonic frequencies derived here are not affected by (near-)instabilities in the reference function.[34,106]

Previously, we reported an average error of 20 cm^{-1} for harmonic frequencies of vibrational stretching modes[34] of diatomic radicals evaluated at the AE-CCSD(T)/cc-pVTZ level of theory, in the absence of (near-)instabilities in the reference. However, the error cancellation between fragments and the supersystem is likely to be significant, because the intrafragment vibrational modes change only slightly upon complexation. Anharmonic normal-mode analysis of the water dimer, using a methodology similar to that applied here, has been reported by Kjærgaard et al.[107] These authors report harmonic vibrational frequencies calculated with FC-CCSD(T)/aug-cc-pVTZ, and VPT2 corrections at the same level of theory. Their results agreed with the experimental ΔE_{ZPVE} to within 0.1 kJ/mol for this system. Nonetheless, it is unclear whether this level of accuracy may be expected for other complexes and whether beneficent error cancellations can always be assumed.

Overall, we estimate the error in the nonrelativistic electronic binding energies, computed on the CCSD(T)/aug-cc-pVTZ geometries, not considering geometric and vibrational effects, to be on the order of 1 kJ/mol. As relativistic contributions to the binding energies are found to be small, errors in the relativistic contributions may contribute only a small amount to the total energetic errors. The error of the real binding energies, accounting for errors in CCSD(T)/aug-cc-pVTZ geometries, zero-point vibrational energies, and relativistic contributions, may be as much as 2−3 kJ/mol.

3.3. Performance of Selected DFT and Wave Function Methods. *Binding Energies Using the Benchmark Geometries.* We assessed the binding energies of selected DFT and wave function methods, employing AE-CCSD(T)/aug-cc-pVTZ geometries throughout. The DFT methods can be roughly grouped into GGAs, SIC-corrected GGAs, hybrid functionals, long-range corrected functionals, and double hybrid functionals. For comparison, results for HF, AE-SOS-MP2, AE-O2-MP2, FC-(RO/U)MP2, FC-CC2, and FC-CCSD methods are reported, as well. The error in binding energy of each method for each complex was calculated as

$$\mathrm{Error}_{i,\mathrm{method}} = E_{i,\mathrm{method}} - E_{i,\mathrm{nonrel}} \tag{11}$$

Errors in predicted binding energies for individual complexes are listed in Table 2. We report the following error statistics: mean signed error ($\bar{\Delta}$), standard deviation (σ), mean absolute error ($\overline{|\Delta|}$), root-mean-square deviation ($\sqrt{\overline{\Delta^2}}$), and root-mean-square percent deviation, defined as

$$\sqrt{\overline{\%\Delta^2}} = \sqrt{\frac{1}{N}\sum_{i}^{N}\left(\frac{E_{i,\mathrm{method}}}{E_{i,\mathrm{CBS}}^{\mathrm{nonrel}}} - 1\right)^2}\cdot 100 \tag{12}$$

Statistics for the entire data set and different subsets are presented in Table 3.

Among the wave function methods inferior to CCSD(T), CCSD (N^6 scaling) is the best performer. CCSD gives binding energies close to the benchmark energies in all cases and exhibits the lowest $\sqrt{\overline{\Delta^2}}$ of all approximate methods (including DFT) tested here. CCSD is more expensive than other methods evaluated here, but recent advances in linear-scaling correlation methods[108] put its application to extended micro-hydrated systems in reach. The MP2 and CC2 (N^5 scaling) methods perform similarly to each other, except for the systems $HF\cdots CO^+$ and $H_2O\cdots F$. For these two complexes, CC2 clearly outperforms MP2. For the heavily spin-contaminated $HF\cdots CO^+$ system, ROMP2 improves upon MP2, which suggests that the problems of MP2 are related to spin contamination for this case. For $H_2O\cdots F$, MP2 and ROMP2 perform equally poorly. In the benchmark calculations, $H_2O\cdots F$ exhibits relatively high perturbative triples (T) and HLC contributions to the binding energy, which is indicative of static correlation. The CC2 method apparently copes with both spin contamination and static correlation to some extent. With an increasing level of excitation in the post-HF treatment (UHF, UMP2, UCC2, and UCCSD), the $\langle S^2\rangle$ values for CO+ decrease (0.97, 0.94, 0.86, and 0.77). With respect to the UHF reference, UCC2 offers some advantage in spin contamination removal compared to UMP2. The improved treatment of static correlation of CC2 can likely be attributed to the inclusion of the singles excitations, similar to CCSD.[104]

The N^4 scaling correlated methods based on the scaled-opposite-spin (SOS) formalism, SOS-MP2 and O2-MP2, show mixed performance compared to conventional MP2. They both perform worse than MP2 for $H_2O\cdots Al$, but O2−MP2 improves the description of both $HF\cdots CO^+$ and $H_2O\cdots F$ compared to MP2. With the exception of CCSD, none of the wave function methods discussed here provide a performance that distinguishes them significantly from the best DFT methods (*vide infra*).

All DFT functionals were used with unrestricted orbitals (UKS), except for the GPW-BLYP calculations, which were performed in a restricted open shell (ROKS) framework. We briefly investigated the UKS/ROKS differences for the hybrid functionals BHandHLYP and MPW1K, both of which bear a high fraction of exact exchange and are somewhat affected by spin contamination. For these two methods, binding energies obtained by the ROKS approach were within 0.2 kJ/mol of the UKS results, except for three of the hemibonded systems, wherein the differences were slightly more pronounced ($H_2O\cdots F$, 2.6; $H_2O\cdots NH_3^+$, 0.6; and $HF\cdots CO^+$, 0.4 kJ/mol). On the basis of these results, we expect ROKS and UKS to yield similar performances for the different functionals tested here, and we do not report binding energies for the respective complementary formalism.

For H-bonded systems, most DFT methods show slight systematic overbinding but provide chemical accuracy, with average errors of <4.2 kJ/mol. The magnitude of errors found agrees well with those reported in a previous study on closed-shell H-bonded systems[75] for the functionals that were evaluated in both assessments (PBE, BLYP, B3LYP). However, some functionals perform significantly worse than others, for example PBE and LC-PBE, LC-BLYP and GPW-BLYP, the latter performing worse than regular BLYP. For the methods to which it was applied, Grimme's dispersion correction had only a minor impact on the results. To our surprise, the performance of GPW-BLYP was worsened when including the self-interaction correction (SIC).

For electron-poor/hemibonded complexes, almost all DFT methods tested overbind. GGAs perform worst, which is consistent with previous reports[23] on $H_2O\cdots NH_3^+$, a system included in our data set. The situation is improved if exact exchange is introduced, but we did not observe a trend relating the performance of different hybrid functionals to the percentage of exact exchange used in the respective functionals. The good performance statistics of the M06 functionals compared to other hybrid functionals is related to their

improved description of the HF···CO^+ complex. However, for the remaining complexes of this group, MPW1K and BHandHLYP perform better than the M06 functionals. The M06HF functional was difficult to converge for the majority of the systems. Compared to GGAs, inclusion of second order perturbative correlation systematically improves hemibonded binding energies, but there is significant variation between the three double hybrids tested. The long-range corrected functionals improve significantly upon GGAs, as well, but some complexes remain overbound. The SIC ameliorates the BLYP overbinding for all complexes except HF···CO^+. Because most methods overbind these electron-poor complexes, we do not expect an empirical dispersion correction to improve the performance, unless the functional is reparametrized alongside, as is done in the case of ωB97XD.

For H_2O···Li and H_2O···Be^+, errors are less systematic than for the electron-deficient hemibonded complexes. In the complexes of these electron-rich radicals, there is no systematic overbinding. Overall, the performance of DFT methods is better for these systems compared to hemibonded complexes, but chemical accuracy is not reached. The long-range corrected functionals exhibit considerable errors for the H_2O···Be^+ system. Across the set of DFT methods tested, errors in the binding energies of H_2O···Be^+ and H_2O···Li are correlated (Pearson correlation coefficient of 0.69). Functionals that show large errors for H_2O···Be^+ and H_2O···Li also show errors for H_2O···Al. However, over all DFT methods considered here, we found no correlation between the errors of H_2O···Al and the errors of H_2O···Li and H2O···Be^+, which suggests differing origins among these errors. The two double hybrids that perform best for hemibonded complexes and the Li/Be^+ complexes, XYG3 and ωB97X-2, both severely overbind the H_2O···Al complex.

On the basis of the data presented above, it is difficult to make general statements about the performances of families of functionals for the test set of radical−solvent complexes considered here. Among the hybrid functionals and the long-range corrected functionals, prediction skill varies widely when applied to the different classes of complexes. For the types of problems tested here, performance varies more among individual functionals than among families of functionals. This suggests that different functional forms may be parametrized to perform well for these problems.

Optimized Geometries and Intermolecular Distances. For the BLYP, PBE, B3LYP, M062X, BHandHLYP, MPW1K, BMK, MPW2PLYP, B2PLYP, B2PLYPD, LC-BLYP, LC-PBE, LC-ωPBE, CAM-B3LYP, ωB97, ωB97X, and ωB97XD functionals, we also optimized the geometries using the aug-cc-pVDZ basis set. That these results are not basis set converged should be kept in mind. We made this choice to estimate accuracy at a level of theory that will likely be used in practice for extended systems. On these geometries, we recomputed binding energies with the aug-cc-pVQZ basis.

DFT-optimized structures agree well with the CCSD(T)/aug-cc-pVTZ structures in most cases (Table S4). The distances between the closest nuclei on the respective fragments are usually within 0.1 Å of the CCSD(T) benchmark structure. Nonetheless, some functionals perform better than others, on average. For example, the long-range corrected functionals provide intermolecular distances inferior to other functionals. Across the methods considered, we did not observe an association between the error in binding energy (Table 2) and the error in intermolecular distance (Table S4). The Pearson correlation coefficients between these two types of errors, over all methods in Table S4, are found to be −0.1 for the signed errors and 0.2 for the unsigned errors.

Few qualitative discrepancies between the DFT and the CCSD(T) structures were observed. For the H_2O···NH_3^+ complex, the NH_3^+ fragment is planar in the CCSD(T) geometry. Using a GGA functional and optimizing the geometry starting from the CCSD(T) structure, the NH_3^+ fragment becomes pyramidalized, even though the N−O distance remains constant. This structure is a transition state on the DFT PES, and requires reorientation of the water hydrogens to reach a minimum. This minimum is, in turn, not present on the coupled cluster PES. The introduction of exact exchange planarizes the NH_3^+ fragment, but none of the tested DFT functionals correctly identifies the CCSD(T) structure as a minimum on their respective PES. However, on each DFT PES, the DFT-optimized structure and the CCSD(T)-optimized structure are within 1 kJ/mol of each other. Hence, for this system, all DFT models yield a qualitatively incorrect geometry. This result may have little practical energetic relevance, but it may serve as a warning, especially for spectroscopic applications.

Discrepancies between DFT binding energies computed on CCSD(T) geometries and those computed on DFT-optimized geometries are typically within 2.5 kJ/mol (Table S5). However, these differences are more pronounced for some of the hemibonded complexes, and reach up to a 12.5 kJ/mol decrease in binding energy for the GGA functionals for the H_2O···NH_3^+ complex. For this "worst case" system, B3LYP (−6.2 kJ/mol) and ωB97XD (−4.2 kJ/mol) show a significant lowering in binding energy, whereas this difference is negligible for the remainder of the functionals. We conclude from the data in Table S5 that DFT binding energies computed using DFT geometries are, for practical purposes, identical with those computed using CCSD(T) geometries, provided that a functional is chosen which performs well for the type of interaction considered.

4. CONCLUSIONS

We present a new database of accurately quantified geometries and binding energies for small doublet radicals interacting with the polar (model) solvent molecules H_2O and HF. We find that FC-CCSD(T)/CBS captures the benchmark binding energy to within chemical accuracy for complexes with electron-rich main-group metals, and to within 1 kJ/mol for the rest of the set. Core−valence correlation and post-CCSD(T) excitations contribute only a small part to the overall binding energy.

The performances of different DFT methods are mixed. Some methods exhibit relative accuracy consistently in the 10−20% range; that is, they have quantitative prediction skill. However, in terms of the absolute binding energy, "chemical accuracy" (1 kcal/mol) is frequently not reached. A general statement on the performance of "classes" of functionals (hybrid, double hybrid, long-range corrected) is not evident. Different members of these families show different levels of accuracy among the different sets of complexes. As an overview, we present a box plot of the binding energy errors for all methods in Figure 2. This plot also shows that the minimal and maximal errors encountered in the present data set are often far from the mean errors. As an example which illustrates the variability that can arise within a family of functionals, consider the performances of long-range corrected functionals for H-

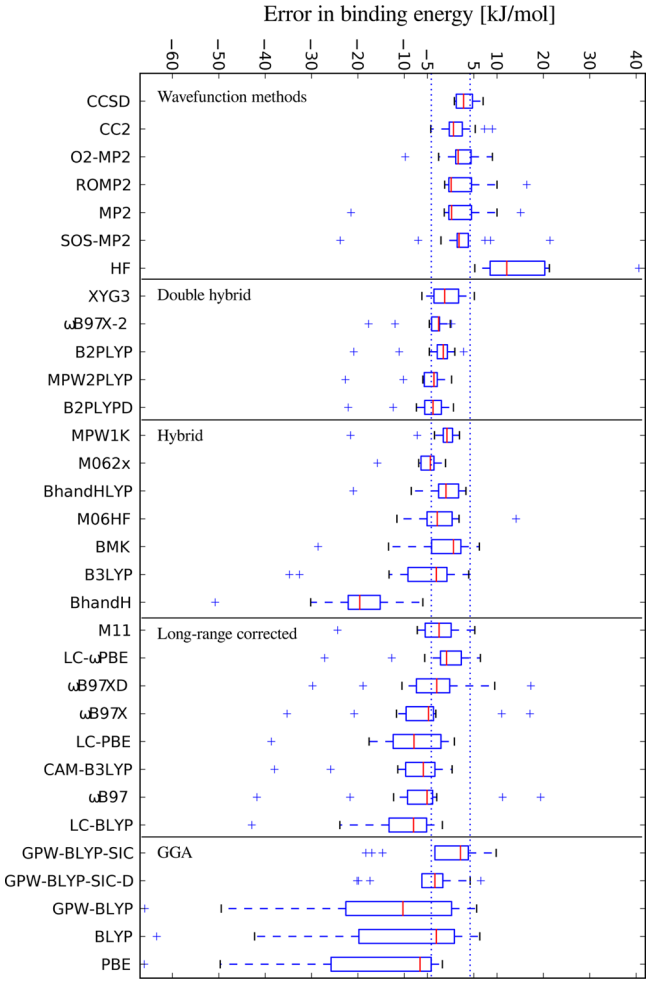

Figure 2. Box plot showing the errors of different wave function and DFT methods for binding energies [kJ/mol]. Red lines denote the median errors, the boxes contain errors from the 25th percentile to the 75th percentile (first (Q1) and third (Q3) quartile). The whiskers denote the lowest datum and highest datum which are still within 1.5× the interquartile range. These limits are defined as Q1 − 1.5 (Q3−Q1) and Q3 + 1.5 (Q3−Q1).[109] Data points outside this range are explicitly shown (crosses). Vertical dotted lines denote "chemical accuracy," or an error of 1 kcal/mol.

bonded systems: only M11 and ωB97XD exhibit accuracy close to the best conventional hybrid functionals.

The largest differences in performance of different functionals can be found for electron-poor/hemibonded complexes. None of the long-range corrected functionals compete with the MPW1K and BHandHLYP hybrid functionals, both of which have been identified previously to perform well for such systems. However, some double hybrid functionals seem to perform significantly better for the systems tested here (ωB97-X2 and XYG3). Using the Perdew−Zunger SIC on the spin density improves the performances of BLYP, and this method is recommended as a cost-effective alternative to hybrid functionals for extended systems.

Among the functionals tested here, the MPW1K functional appears the most robust across binding types. This functional also performs reasonably well for reaction barriers,[88] although in other areas it is outperformed by more recent functionals.[82,84] Hence, we think that there may still be room for the development and improvement of functionals that can describe radical chemistry, as well as other areas equally well. The benchmark data presented here may enable testing and/or parametrization of such functionals.

■ ASSOCIATED CONTENT

Supporting Information

The following data are available: Tables describing the influence of basis-set incompleteness and counterpoise correction on interfragment distances; tables containing the errors in interfragment distances of DFT geometries with respect to AE-CCSD(T)/aug-cc-pVTZ geometries and impact on the associated binding energies; Z-matrices for all complexes optimized at the AE-CCSD(T)/aug-cc-pVTZ level of theory and AE-CCSD(T)/aug-cc-pCVQZ level of theory. This material is available free of charge via the Internet at http://pubs.acs.org/.

■ AUTHOR INFORMATION

Corresponding Author

*E-mail: samuel.arey@epfl.ch.

Notes

The authors declare no competing financial interest.

■ ACKNOWLEDGMENTS

This work was supported by the Swiss National Science Foundation (SNSF) ProDoc TM Grant PDFMP2-123028.

■ REFERENCES

(1) Zhao, J.; Zhang, R. *Adv. Quantum Chem.* **2008**, *55*, 177−213.
(2) Maciel, G. S.; Cappelletti, D.; Grossi, G.; Pirani, F.; Aquilanti, V. *Adv. Quantum Chem.* **2008**, *55*, 311−332.
(3) Glowacki, D. R.; Pilling, M. J. *ChemPhysChem* **2010**, *11*, 3836−3843.
(4) Francisco, J. S.; Muckerman, J. T.; Yu, H.-G. *Acc. Chem. Res.* **2010**, *43*, 1519−1526.
(5) Canonica, S.; Tratnyek, P. *Environ. Toxicol. Chem.* **2003**, *22*, 1743−54.
(6) Coote, M. L. *Macromol. Theory Simul.* **2009**, *18*, 388−400.
(7) Augusto, O.; Bonini, M. G.; Amanso, A. M.; Linares, E.; Santos, C. C.; Menezes, S. L. D. *Free Radical Biol. Med.* **2002**, *32*, 841−859.
(8) Galano, A.; Alvarez-Idaboyb, J. R. *Adv. Quantum Chem.* **2008**, *55*, 245−274.
(9) Iuga, C.; Alvarez-Idaboy, J. R.; Reyes, L.; Vivier-Bunge, A. *J. Phys. Chem. Lett.* **2010**, *1*, 3112−3115.
(10) Buszek, R. J.; Francisco, J. S.; Anglada, J. M. *Int. Rev. Phys. Chem.* **2011**, *30*, 335−369.
(11) Hashimoto, K.; Daigoku, K. *Phys. Chem. Chem. Phys.* **2009**, *11*, 9391−9400.
(12) Cwiklik, L.; Buck, U.; Kulig, W.; Kubisiak, P.; Jungwirth, P. *J. Chem. Phys.* **2008**, *128*, 154306.
(13) Liu, H. T.; Müller, J. P.; Zhavoronkov, N.; Schulz, C. P.; Hertel, I. V. *J. Phys. Chem. A* **2010**, *114*, 1508−1513.
(14) Salter, T. E.; Mikhailov, V.; Ellis, A. M. *J. Phys. Chem. A* **2007**, *111*, 8344−8351.
(15) Peng, X.; Kong, W. *J. Chem. Phys.* **2002**, *117*, 9306−9315.
(16) Forysinski, P. W.; Zielke, P.; Luckhaus, D.; Corbett, J.; Signorell, R. *J. Chem. Phys.* **2011**, *134*, 094314.
(17) Otto, R.; Brox, J.; Trippel, S.; Stei, M.; Best, T.; Wester, R. *Nat. Chem.* **2012**, *4*, 534−538.
(18) Chałasiński, G.; Szczęśniak, M. M. *Chem. Rev.* **2000**, *100*, 4227−4252.
(19) Rudic, S.; Merritt, J. M.; Miller, R. E. *Phys. Chem. Chem. Phys.* **2009**, *11*, 5345−5352.
(20) Sander, W.; Roy, S.; Polyak, I.; Ramirez-Anguita, J. M.; Sanchez-Garcia, E. *J. Am. Chem. Soc.* **2012**, *134*, 8222−8230.
(21) Gill, P. M. W.; Radom, L. *J. Am. Chem. Soc.* **1988**, *110*, 4931−4941.

(22) Bickelhaupt, F. M.; Diefenbach, A.; de Visser, S. P.; de Koning, L. J.; Nibbering, N. M. M. *J. Phys. Chem. A* **1998**, *102*, 9549−9553.
(23) Kim, H.; Lee, H. M. *J. Phys. Chem. A* **2009**, *113*, 6859−6864.
(24) Lee, H. M.; Kim, K. S. *J. Chem. Theory Comput.* **2009**, *5*, 976−981.
(25) Bil, A.; Berski, S.; Latajka, Z. *J. Chem. Inf. Model.* **2007**, *47*, 1021−1030.
(26) Burcl, R.; Hobza, P. *Theor. Chem. Acc.* **1993**, *87*, 97−105.
(27) Hobza, P.; Burcl, R.; Špirko, V.; Dopfer, O.; Müller-Dethlefs, K.; Schlag, E. W. *J. Chem. Phys.* **1994**, *101*, 990−997.
(28) Sodupe, M.; Oliva, A.; Bertran, J. *J. Am. Chem. Soc.* **1994**, *116*, 8249−8258.
(29) Coitiño, E. L.; Lledos, A.; Serra, R.; Bertran, J.; Ventura, O. N. *J. Am. Chem. Soc.* **1993**, *115*, 9121−9126.
(30) Coitiño, E. L.; Pereira, A.; Ventura, O. N. *J. Chem. Phys.* **1995**, *102*, 2833−2840.
(31) Humbel, S.; Côte, I.; Hoffmann, N.; Bouquant, J. *J. Am. Chem. Soc.* **1999**, *121*, 5507−5512.
(32) Stanton, J. F.; Gauss, J. *Adv. Chem. Phys.* **2003**, *125*, 101−146.
(33) Szalay, P. G.; Vázquez, J.; Simmons, C.; Stanton, J. F. *J. Chem. Phys.* **2004**, *121*, 7624−7631.
(34) Tentscher, P. R.; Arey, J. S. *J. Chem. Theory Comput.* **2012**, *8*, 2165−2179.
(35) d'Auria, R.; Kuo, I.-F. W.; Tobias, D. J. *J. Phys. Chem. A* **2008**, *112*, 4644−4650.
(36) Grafenstein, J.; Kraka, E.; Cremer, D. *Phys. Chem. Chem. Phys.* **2004**, *6*, 1096−1112.
(37) Grüning, M.; Gritsenko, O. V.; van Gisbergen, S. J. A.; Baerends, E. J. *J. Phys. Chem. A* **2001**, *105*, 9211−9218.
(38) Ruiz, E.; Salahub, D. R.; Vela, A. *J. Phys. Chem.* **1996**, *100*, 12265−12276.
(39) Steinmann, S. N.; Piemontesi, C.; Delachat, A.; Corminboeuf, C. *J. Chem. Theory Comput.* **2012**, *8*, 1629−1640.
(40) Perdew, J. P.; Zunger, A. *Phys. Rev. B* **1981**, *23*, 5048−5079.
(41) VandeVondele, J.; Sprik, M. *Phys. Chem. Chem. Phys.* **2005**, *7*, 1363−1367.
(42) d'Avezac, M.; Calandra, M.; Mauri, F. *Phys. Rev. B* **2005**, *71*, 205210.
(43) Janesko, B. G.; Henderson, T. M.; Scuseria, G. E. *J. Chem. Phys.* **2009**, *131*, 034110.
(44) Yanai, T.; Tew, D. P.; Handy, N. C. *Chem. Phys. Lett.* **2004**, *393*, 51−57.
(45) Iikura, H.; Tsuneda, T.; Yanai, T.; Hirao, K. *J. Chem. Phys.* **2001**, *115*, 3540−3544.
(46) Braïda, B.; Hiberty, P. C.; Savin, A. *J. Phys. Chem. A* **1998**, *102*, 7872−7877.
(47) Pople, J. A.; Nesbet, R. K. *J. Chem. Phys.* **1954**, *22*, 571−572.
(48) Salter, E. A.; Trucks, G. W.; Bartlett, R. J. *J. Chem. Phys.* **1989**, *90*, 1752−1766.
(49) Stanton, J. F.; Gauss, J. *J. Chem. Phys.* **1994**, *101*, 8938−8944.
(50) Nooijen, M.; Bartlett, R. J. *J. Chem. Phys.* **1995**, *102*, 3629−3647.
(51) Watts, J. D.; Gauss, J.; Bartlett, R. J. *Chem. Phys. Lett.* **1992**, *200*, 1−7.
(52) Stanton, J. F.; Gauss, J.; Harding, M. E.; Szalay, P. G. with contributions from Auer, A. A.; Bartlett, R. J.; Benedikt, U.; Berger, C.; Bernholdt, D. E.; Bomble, Y. J.; Cheng, L.; Christiansen, O.; Heckert, M.; Heun, O.; Huber, C.; Jagau, T.-C.; Jonsson, D.; Jusélius, J.; Klein, K.; Lauderdale, W. J.; Matthews, D. A.; Metzroth, T.; Mück, L. A.; O'Neill, D. P.; Price, D. R.; Prochnow, E.; Puzzarini, C.; Ruud, K.; Schiffmann, F.; Schwalbach, W.; Stopkowicz, S.; Tajti, A.; Vázquez, J.; Wang, F.; Watts, J. D. and the integral packages *MOLECULE* (Almlöf, J.; Taylor, P. R.), *ABACUS* (Helgaker, T.; Jensen, H. J. Aa.; Jørgensen, P.; Olsen, J.), and *ECP* routines (Mitin, A. V.; van Wüllen, C.). For the current version, see http://www.cfour.de (accessed October 2011).
(53) Watts, J. D.; Bartlett, R. J. *J. Chem. Phys.* **1990**, *93*, 6104−6105.
(54) Bomble, Y. J.; Stanton, J. F.; Kállay, M.; Gauss, J. *J. Chem. Phys.* **2005**, *123*, 054101.
(55) Oliphant, N.; Adamowicz, L. *J. Chem. Phys.* **1991**, *95*, 6645−6651.
(56) MRCC, a string-based quantum chemical program suite written by M. Kállay. See also: Kállay, M.; Surján, P. R. *J. Chem. Phys.* **2001**, *115*, 2945 as well as www.mrcc.hu (accessed October 2011).
(57) DeYonker, N. J.; Peterson, K. A.; Wilson, A. K. *J. Phys. Chem. A* **2007**, *111*, 11383−11393.
(58) Kendall, R. A.; Dunning, T. H., Jr.; Harrison, R. J. *J. Chem. Phys.* **1992**, *96*, 6796−6806.
(59) Peterson, K. A.; Dunning, T. H., Jr. *J. Chem. Phys.* **2002**, *117*, 10548−10560.
(60) Dunning, T. H., Jr. *J. Chem. Phys.* **1989**, *90*, 1007−1023.
(61) Woon, D. E.; Dunning, T. H., Jr. *J. Chem. Phys.* **1993**, *98*, 1358−1371.
(62) Woon, D. E.; Dunning, T. H., Jr. *J. Chem. Phys.* **1995**, *103*, 4572−4585.
(63) Szalay, P. G.; Gauss, J.; Stanton, J. F. *Theor. Chem. Acc.* **1998**, *100*, 5−11.
(64) Schneider, W.; Thiel, W. *Chem. Phys. Lett.* **1989**, *157*, 367−373.
(65) Frisch, M. J. et al. *Gaussian 09*, Revision B.1; Gaussian Inc.: Wallingford, CT, 2009.
(66) Boys, S.; Bernardi, F. *Mol. Phys.* **1970**, *19*, 553−566.
(67) Simon, S.; Duran, M.; Dannenberg, J. J. *J. Chem. Phys.* **1996**, *105*, 11024−11031.
(68) Halkier, A.; Helgaker, T.; Jørgensen, P.; Klopper, W.; Koch, H.; Olsen, J.; Wilson, A. K. *Chem. Phys. Lett.* **1998**, *286*, 243−252.
(69) Schwenke, D. W. *J. Chem. Phys.* **2005**, *122*, 014107.
(70) Cowan, R. D.; Griffin, D. C. *J. Opt. Soc. Am.* **1976**, *66*, 1010−1014.
(71) Klopper, W. *J. Comput. Chem.* **1997**, *18*, 20−27.
(72) Faas, S.; Snijders, J.; van Lenthe, J.; van Lenthe, E.; Baerends, E. *Chem. Phys. Lett.* **1995**, *246*, 632−640.
(73) Valiev, M.; Bylaska, E.; Govind, N.; Kowalski, K.; Straatsma, T.; Dam, H. V.; Wang, D.; Nieplocha, J.; Apra, E.; Windus, T.; de Jong, W. *Comput. Phys. Commun.* **2010**, *181*, 1477−1489.
(74) Nichols, P.; Govind, N.; Bylaska, E.; de Jong, W. *J. Chem. Theory Comput.* **2009**, *5*, 491−499.
(75) Boese, A. D.; Martin, J. M. L.; Klopper, W. *J. Phys. Chem. A* **2007**, *111*, 11122−11133.
(76) Boese, A. D.; Oren, M.; Atasoylu, O.; Martin, J. M. L.; Kállay, M.; Gauss, J. *J. Chem. Phys.* **2004**, *120*, 4129−4141.
(77) Martin, J. M. L.; de Oliveira, G. *J. Chem. Phys.* **1999**, *111*, 1843−1856.
(78) Miehlich, B.; Savin, A.; Stoll, H.; Preuss, H. *Chem. Phys. Lett.* **1989**, *157*, 200−206.
(79) Becke, A. D. *J. Chem. Phys.* **1996**, *104*, 1040−1046.
(80) Grimme, S. *J. Chem. Phys.* **2006**, *124*, 034108.
(81) Schwabe, T.; Grimme, S. *Phys. Chem. Chem. Phys.* **2007**, *9*, 3397−3406.
(82) Zhao, Y.; Truhlar, D. *Theor. Chem. Acc.* **2008**, *120*, 215−241.
(83) Zhao, Y.; Truhlar, D. G. *J. Phys. Chem. A* **2006**, *110*, 13126−13130.
(84) Boese, A. D.; Martin, J. M. L. *J. Chem. Phys.* **2004**, *121*, 3405−3416.
(85) Perdew, J. P.; Burke, K.; Ernzerhof, M. *Phys. Rev. Lett.* **1996**, *77*, 3865−3868.
(86) Perdew, J. P.; Burke, K.; Ernzerhof, M. *Phys. Rev. Lett.* **1997**, *78*, 1396−1396.
(87) Becke, A. D. *J. Chem. Phys.* **1993**, *98*, 1372−1377.
(88) Lynch, B. J.; Fast, P. L.; Harris, M.; Truhlar, D. G. *J. Phys. Chem. A* **2000**, *104*, 4811−4815.
(89) Schwabe, T.; Grimme, S. *Phys. Chem. Chem. Phys.* **2006**, *8*, 4398−4401.
(90) Chai, J.-D.; Head-Gordon, M. *J. Chem. Phys.* **2008**, *128*, 084106.
(91) Chai, J.-D.; Head-Gordon, M. *Phys. Chem. Chem. Phys.* **2008**, *10*, 6615−6620.
(92) Vydrov, O. A.; Scuseria, G. E. *J. Chem. Phys.* **2006**, *125*, 234109.
(93) Shao, Y.; et al. *Phys. Chem. Chem. Phys.* **2006**, *8*, 3172−3191.
(94) Peverati, R.; Truhlar, D. G. *J. Phys. Chem. Lett.* **2011**, *2*, 2810−2817.

(95) Zhang, Y.; Xu, X.; Goddard, W. A. *Proc. Natl. Acad. Sci. U. S. A.* **2009**, *106*, 4963−4968.
(96) Chai, J.-D.; Head-Gordon, M. *J. Chem. Phys.* **2009**, *131*, 174105.
(97) VandeVondele, J.; Krack, M.; Mohamed, F.; Parrinello, M.; Chassaing, T.; Hutter, J. *Comput. Phys. Commun.* **2005**, *167*, 103−128.
(98) Krack, M. *Theor. Chem. Acc.* **2005**, *114*, 145−152.
(99) Grimme, S. *J. Comput. Chem.* **2006**, *27*, 1787−1799.
(100) Christiansen, O.; Koch, H.; Jørgensen, P. *Chem. Phys. Lett.* **1995**, *243*, 409−418.
(101) Jung, Y.; Lochan, R. C.; Dutoi, A. D.; Head-Gordon, M. *J. Chem. Phys.* **2004**, *121*, 9793−9802.
(102) Lochan, R. C.; Head-Gordon, M. *J. Chem. Phys.* **2007**, *126*, 164101.
(103) Shepler, B. C.; Wright, A. D.; Balabanov, N. B.; Peterson, K. A. *J. Phys. Chem. A* **2007**, *111*, 11342−11349.
(104) Helgaker, T.; Jørgensen, P.; Olsen, J. *Molecular Electronic Structure Theory*; Wiley: New York, 2004; pp 817−883.
(105) Karton, A.; Taylor, P. R.; Martin, J. M. L. *J. Chem. Phys.* **2007**, *127*, 064104.
(106) Crawford, T. D.; Stanton, J. F.; Allen, W. D.; Schaefer, H. F., III. *J. Chem. Phys.* **1997**, *107*, 10626−10632.
(107) Kjærgaard, H. G.; Garden, A. L.; Chaban, G. M.; Gerber, R. B.; Matthews, D. A.; Stanton, J. F. *J. Phys. Chem. A* **2008**, *112*, 4324−4335.
(108) Ziółkowski, M.; Jansík, B.; Kjærgaard, T.; Jørgensen, P. J. *Chem. Phys.* **2010**, *133*, 014107.
(109) In normally distributed data, the median is equivalent to the mean, the box is equivalent to $\pm$ 0.67σ, and the whiskers are equivalent to $\pm$ 2.70σ.